# Impact of Suprathermal Ions on Neutron Yield at Pre-DT Phase of ITER Operation

A.R. Polevoi[1], A. Loarte[1], R. Bilato[2], N. Gorelenkov[3], Ye.O. Kazakov[4], E. Polunovskiy[1], A. Tchistiakov[1], E. Fable[2], V. Kiptily[5], A.V. Krasilnikov[6], A.Y. Kuyanov[7], R. Nazikian[3], S.D. Pinches[1], M. Schneider[1]

[1]*ITER Organization, Route de Vinon-sur-Verdon, CS90046, 13067 St Paul-lez-Durance, France*

[2]*Max-Planck Institut für Plasmaphysik, D-85748 Garching, Germany*

[3]*PPPL, PO Box 451, Princeton, NJ 08543, USA*

[4]*Laboratory for Plasma Physics, LPP-ERM/KMS, Brussels, Belgium*

[5]*CCFE, Culham Science Centre, Abingdon OX14 3DB, United Kingdom*

[6]*Institution "Project Center ITER", 123098 Moscow, Russian Federation*

[7]*NRC Kurchatov Institute, 123098 Moscow, Russian Federation*

**Abstract**

An assessment of neutron production during the Pre-Fusion Power Operation (PFPO) phase has been carried out for a representative set of plasma scenarios foreseen by the ITER Research Plan. A range of heating systems, namely NBI (hydrogen), ECRH and ICRH, are planned to be used for the PFPO studies in helium, hydrogen and mixed hydrogen-helium plasmas. Fast ions (protons and $^3$He) originating from NBI and ICRH systems can increase neutron production in PFPO plasmas by directly interacting with intrinsic Be impurities or through the secondary processes, as also evidenced on JET. Generation of fast ions in ITER PFPO scenarios has been modelled using the ASTRA-NBI and TORIC-SSFPQL codes. A significant impact of a synergy between the hydrogen NBI and hydrogen minority ICRH on neutron production in helium plasmas is reported. In addition, the stability of the toroidicity-induced Alfvén eigenmodes (TAE) is analysed for PFPO plasmas with a high pressure of suprathermal ions and a weak reversed shear. The possible impact of sawtooth oscillations and TAEs on the neutron production is discussed, based on linear stability analysis.

## 1. Introduction

The production of neutrons in the Pre-Fusion Power Operation (PFPO) of the ITER Research Plan (IRP) is foreseen to be very low compared to Fusion Power Operation (FPO) phase in which DT burning plasmas with high fusion gain will be demonstrated. However, an assessment of its magnitude and of the associated tritium production needs to be performed in view of the plans for commissioning and operation of the heating systems to execute the ITER IRP in the PFPO phase [1].

The assessment of neutron production for pre-DT ITER plasmas was already addressed earlier [2], where the simplified Stix approximation for fast ion distribution functions and fixed plasma parameters $n=10^{20}m^{-3}$, T=10 keV were used. The consideration was limited only to primary reactions of the fast particles accelerated by Hydrogen Neutral Beam Injection ($H^0$-NBI) and Ion Cyclotron Resonance Heating (ICRH) with beryllium impurities, intrinsic in ITER. In addition, the plasma parameters used in [2] are closer to those expected for the ITER baseline 15 MA Q=10 DT-scenario. To ensure robust H-mode access and sustainment, lower plasma densities are envisaged for the PFPO plasmas in ITER. Under these conditions, the population of the fast ion tail can be much higher, which in turn leads to a higher neutron production. Other important effects not considered in Ref. [2] include secondary reactions of fast ions with

Be impurities and synergies between $H^0$-NBI and ICRH hydrogen minority heating in ITER helium plasmas [3], which have a strong impact on the distribution of fast protons and require self-consistent modelling.

In this paper, we thus reassess neutron production during PFPO-1 and PFPO-2 phases, using the expected plasma parameters for the set of scenarios foreseen by the IRP. Profiles of plasma parameters are calculated self-consistently with heating and current-drive sources by 1.5D transport simulations in the ASTRA framework [9]. Electron cyclotron resonance heating (ECRH) and current drive is calculated with the OGRAY code [8]. The distribution function of NBI ions is computed with ASTRA-NBI [4, 5]. The beam energy and NBI power are adjusted to provide acceptable shine-through power loads on ITER's first wall. The ICRH power deposition and distribution function of ICRH-generated fast ions are modelled with the TORIC-SSFPQL suite of codes [6], which also allows studying the synergetic effects between the NBI and ICRH. The synergetic effects are particularly important for scenarios in helium plasmas, where reactions between fast protons and Be impurities produce deuterons and alphas, and then tritium ions and neutrons in secondary reactions.

The outline of the paper is as follows: in section 2, we describe the reactions used in our simulations. We address the secondary reactions induced by fast deuterons and alphas originating from Be-proton reactions and discuss the impact of the fast deuterium spectrum on the secondary reactions. In section 3, we describe the transport models used in our simulations. In section 4, we assess the reaction products for hydrogen and helium plasmas with ECRH and NBI heating only for L- and H-mode scenarios at 1.8/2.65/5.3 T as foreseen for the PFPO phase of the ITER Research Plan. In section 5, we analyze the impact of ICRH on neutron production including the H and $^3$He minority heating schemes, the 3-ion heating scheme and synergetic effects connected with the simultaneous application $H^0$-NBI and ICRH. In section 6, we assess the TAE stability of the PFPO scenarios and discuss the impact of the saw-tooth oscillations and TAE excitation on the neutron yield. We perform AE stability analysis of PFPO plasmas using the perturbative NOVA/NOVA-K suite of codes with rich kinetic physics [10, 11]. In section 7, we discuss the results and summarize our studies.

## 2. Fusion reactions between fast ions and beryllium impurities in ITER plasmas

The relevant reactions for neutron production between $^9$*Be* impurities and fast ions in ITER plasmas are:

$$^9\mathrm{Be}+\mathrm{p} = \mathrm{d}+2\alpha,\ (Q=0.65\ \mathrm{MeV}), \quad (1)$$

$$^9\mathrm{Be}+\mathrm{d} = \mathrm{n}+\mathrm{X}, \quad (2)$$

$$^9\mathrm{Be}+\mathrm{p} = {}^9\mathrm{B}+\mathrm{n}+\gamma, \quad (3)$$

$$^9\mathrm{Be}+{}^3\mathrm{He} = \mathrm{n}+\mathrm{X}, \quad (4)$$

$$^9\mathrm{Be}+\mathrm{p} = {}^6\mathrm{Li}+\alpha\ (Q=2.12\ \mathrm{MeV}), \quad (5)$$

$$^9\mathrm{Be}+\alpha = \mathrm{n}+\mathrm{X}. \quad (6)$$

The cross sections for these reactions available in the nuclear databases (JENDL, TENDL, FENDL, EXFOR and NEA) as recommended by IAEA experts [12] are presented in Fig.1.

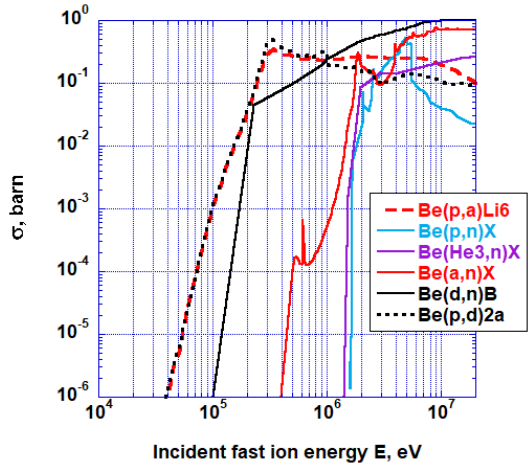


*Figure 1. Cross sections for interaction of fast ions with $Be^9$ impurity as a function of the fast particle incident energy in the laboratory frame*

The cross sections of the secondary reactions (2), (6) strongly depend on the fast d and α energy in the laboratory frame. In the case of ITER, the energy of fast protons originating from the NBI ($E_p \sim 870$ keV) and accelerated by ICRH is comparable with the energy of the reaction products in the primary reactions (1), (5). Therefore, to assess neutron production in the secondary reaction it is necessary to calculate the fast d and α energy spectrum taking into account the fast proton energy in the primary reactions (1), (5).

For a reaction 2(1, 3)4 where particles 1, 2, are the projectile ($p$), target ($^9Be$), and 3, 4 are products, respectively, the energy of particle 3 using non-relativistic kinematics is [13]:

$$E_3 = \frac{m_4}{m_3+m_4}(Q+K) + V\cos\vartheta\sqrt{\frac{2m_3m_4}{m_3+m_4}(Q+K)} + \frac{m_3V^2}{2}, \qquad (7)$$

where $Q$ is the exothermic reaction energy, $K = m_1m_2v^2/(m_1+m_2)/2$ is the relative kinetic energy, $v = v_1 - v_2$ is the relative velocity, $V = (m_1v_1+m_2v_2)/(m_1+m_2)$, is the centre-of-mass (cm) velocity, and $\vartheta$ is the angle between $V$ and the cm velocity of particle 3. Note, that in the cold Be approximation, $K = E_p\, m_2/(m_1+m_2)$, $v = v_p = (2\,E_p/m_1)^{0.5}$, $V = v_p m_1/(m_1+m_2)$.

Thus, Eq (7) for fast d and fast α from reactions (1), (5) takes the form:

$$E_d = 0.8\left(Q+0.9E_p\right) + 0.8\cos\vartheta\sqrt{\left(Q+0.9E_p\right)E_p/10 + 0.02E_p} =$$

$$= 0.8\,Q + 0.74E_p + 0.24\cos\vartheta\sqrt{\left(\frac{Q}{0.9}+E_p\right)E_p}, \qquad (8a)$$

$$E_\alpha = 0.6\left(Q+0.9E_p\right) + 0.4\cos\vartheta\sqrt{0.6\left(Q+0.9E_p\right)E_p + 0.4E_p} =$$

$$\approx 0.6\,Q + 0.94E_p + 0.31\cos\vartheta\sqrt{\left(Q+0.9E_p\right)E_p}. \qquad (8b)$$

Note that for the low energies of $H^0$-NBI- and ICRH-accelerated ions ($E_p \ll Q$) typical for present experiments, the energy of the fast ions, $E_d \approx 0.8\,Q = 0.52\,MeV$, $E_\alpha \approx 0.6\,Q = 1.272\,MeV$, is in the range, where the cross sections of the secondary reactions (2), (6) are small (Fig. 1). For the case of the ITER $H^0$-NBI $E_p = 0.5 - 0.87\,MeV$, and for the hydrogen minority ICRH scheme in ITER, the energy of the proton tail is much higher leading to much higher $d$ and $\alpha$ energies (Eqs. (8a) and (8b)). This has a strong impact on the secondary neutron production in reactions (2), (6), because the resulting $d$ and $\alpha$ energies are in a range where the cross-sections strongly increase.

In further consideration we will distinguish fusion rate, a number of particles of a reaction per second, *S*, and fusion source, a volumetric density of fusion rate, $S'$ = d*S*/d*V*. Taking into account high thresholds of considered reactions (1)-(6) (see figure 1) we describe interaction of fast and thermal particles in the cold ion approximation, neglecting the finite temperatures of thermal ions. The source of fast particles *b3* due to interaction of target Be with fast ions *b2* in reactions ((1) - (6) Be(*b2*,*b3*)X can be expressed as follows:

$$S'_{b3,Beb2} = n_{Be}\int f_{b2}\sigma_{Beb2b3}(E_{b2})v_{b2}d^3\boldsymbol{v}_{b2}, \qquad (9)$$

where: *b2*,*b3* correspond to the relevant fast particles for the reaction, $f_{b2}$is a gyro averaged distribution function of fast ions, produced by NBI, produced in fusion reactions and accelerated by ICRH, which provides the source of the fast particle *b2*, $E_b = m_b v_b^2/2$, $\sigma_{Beb2b3}(E_{b2})$ is the cross section for the reaction of fast ions, *b2* with cold beryllium leading to the creation of fast particle species *b3*, $\int d^3\boldsymbol{v_p}$ corresponds to integration over the velocity space. To calculate fast ion distribution function for an ion specie and to understand the neutron yield dependencies on plasma parameters the general expression (9) can be simplified taking into account features of plasma parameters. In the reactor scale tokamaks with high magnetic field, deviation of the fast ion orbit from the magnetic surface is small relative to gradient length of plasma parameters. This enables using of thin orbit approximation. In this approximation, small densities of fast particles, $n_b/n_e \ll 1$, the gyro averaged distribution function, $f_b$ can be found as a solution of the linearized Fokker-Plank equation (FPE) on a magnetic surface, which has the following general form:

$$\frac{\partial f_b}{\partial t} = L_{coll}(f_b) + L_{QL}(f_b) + S'_b(X,t)\delta(\vec{\boldsymbol{v}}_{b0}) - f_b\sigma_{Beb}(v)n_{Be},$$

where $L_{coll}$ [4],[5] and $L_{QL}$ [6] are differential operators in the velocity space which describe collisions of fast ions with the bulk plasma species, and interaction with RF waves, $S'_b(v,X,t)$ is the fast particle source from the NBI and fusion reactions (1), (5), $f_b\sigma_{Beb}(v)n_{Be}$ is the fast ion sink due to fusion reaction, $\int \delta d^3\boldsymbol{v} = 1$, $\vec{\boldsymbol{v}}_{b0}$, is a speed of a fast ion at birth.

As soon as for cold ion approximation interaction does not depend on the angles, we can use in (9) $\int \ldots d^3\boldsymbol{v} = \int_0^\infty \ldots v^2 dv$, assuming that $f_b$ is gyro and pitch angle averaged solution of the FPE:

$$S'_{b3,Beb2} = c_{Be}n_e\int_0^\infty f_{b2}\sigma_{Beb2b3}(E_{b2})v_{b2}^3 dv_{b2}, \qquad (9.1)$$

We consider the solution of the time-dependent FPE, $f_b(\boldsymbol{v},X,t)$ only in the section 6 to estimate the impact of transients on the neutron yield. For typical ITER parameters fast ion slowing down time is much smaller than the discharge duration [4], and burn out time, $\tau_{fus,b} \equiv (\sigma_{Beb}(v)n_{Be})^{-1}$ : $\tau_{sb} \ll 100$ s, $\tau_{sb} \ll (\sigma_{Beb}(v)n_{Be})^{-1}$, where $\tau_{sb} \approx 2A_bT_e^{3/2}Z_b^{-4}n_e^{-1}/ln\Lambda, A_b = m_b/m_b$, Thus we can neglect the sink, $f_b\sigma_{Beb}(v)n_{Be}$, and for further analyses, except section 6, we can use solution of the stationary FPE with $\partial f_b/\partial$t=0.

For secondary reactions and fast protons from NBI it is possible to use the slow-down approximation for solution of the stationary FPE, $L_{coll}(f_b) + S'_b(X)\delta(\vec{\boldsymbol{v}}_{b0}) = 0$, which sufficiently accurate reproduced the fast ion distribution of the velocity space in the high energy range of interest:

$$S'_{b3,Beb2} = S'_{b2}\left(E_{b2,0}\right)c_{Be}\int_0^{E_{b2,0}}\frac{\tau_{sb2}n_e}{v^3+v_{cb2}^3}\sigma_{Beb2b3}(E)v^3dv, \quad (10)$$

where the slowing down distribution function looks like:

$$f_b\left(T_e,n_e,v,E_{b,0}\right) = S'_b\left(E_{b,0}\right)\frac{\tau_{sb}}{v^3+v_{cb}^3}H\left(E-E_{b,0}\right), \quad (11)$$

where $(v_c/v_{b0}\,)^2 \approx 14.8T_e m_b \Sigma m_i^{-1} n_i Z_i^2/E_{b,0}/n_e$, $E_{b,0}$, is the energy of an ion at born, *H* is the Heaviside function.

Note that function

$$F_{b3,Beb2}(E_{be2},T) = S'_{b3,Beb2}/S'_{b2}\left(E_{b2,0}\right)c_{Be} = \int_0^{E_{b2,0}}\frac{\tau_{sb2}n_e}{v^3+v_{cb2}^3}\sigma_{Beb2b3}(E)v^3dv \quad (12)$$

depends on density just logarithmically, ($\sim 1/ln\Lambda$). Then, hereafter we refer to $F_{b3,Beb2}$ as a relative probability of the source of fast ions *b2*, $S'_{b2}\left(E_{b2,0}\right)$, to convert to the source of the fusion products *b3*, $S'_{b3,Beb2}$.Then the probability of such conversion can be expressed as $S'_{b3,Beb2}/S'_{b2}\left(E_{b2,0}\right) = c_{Be}F_{b3,Beb2}(E_{be2},T)$. Thus, $S'_{b3,Beb2} = S'_{b2}\left(E_{b2,0}\right)c_{Be}F_{b3,Beb2}(E_{be2},T)$

Sources of the fast ions involved in the secondary reactions with the thermal ions A=Be, D, T depend on the primary fast ion source energy, $E_{b2}$ , and angle of velocities of the produced ions, $\vartheta$, (see Eqs. (7), (8)): $S'_{b3,Ab2}(E_{b3}(E_{b2},\vartheta))$. Thus, the distribution function of the secondary ions has the form:

$$f_{b3}\left(T_e,n_e,v,E_{b3}(E_{b2,0},\vartheta)\right) = S'_{b3}(E_{b3}(E_{b2,0},\vartheta))\frac{\tau_{sb3}}{v^3+v_{cbs}^3}H(E-E_{b3}).$$

Then, assuming homogeneous distribution of secondary ions over the angle $\vartheta$

Then the ion source of secondary reaction can be expressed as the averaged over the angle Assuming homogeneous angle ($\vartheta$) directivity of fast ions produced in the primary reactions (see eqs. (7), (8)), for the ion source for the secondary reactions one has:

$$S'_{b4,Ab3} = \{S'_{b3,Beb2}(E_{b3}(E_{b2},\vartheta))c_{Be}\int_0^{E_{b3}}\frac{\tau_{sb3}n_e}{v^3+v_{cb3}^3}\sigma_{Ab3b4}(E)v^3dv\} =$$
$$= S'_{b2}\left(E_{b2,0}\right)c_A c_{Be}F_{b3,A}(E_{be2},T),$$

where *b4* is the fast particle specie, produced in the secondary reaction with ions from the primary reaction of thermal ions with fast particles,

$$F_{b3,A}(E_{be2},T) = F_{b3,Beb2}(E_{be2},T)\{\int_0^{E_{b3}}\frac{\tau_{sb3}n_e}{v^3+v_{cb3}^3}\sigma_{Ab3b4}(E)v^3dv\}, \quad (13)$$

where brackets {…} notes the averaging over the angle $\vartheta$, assuming homogeneous distribution of the secondary ions (see eqs. (8)). Functions $F_{b3,Beb2}(E_{be2},T)$ and $F_{b3,A}(E_{be2},T)$ correspond to relative probabilities of conversion of the original fast protons into the fusion products *b3*.

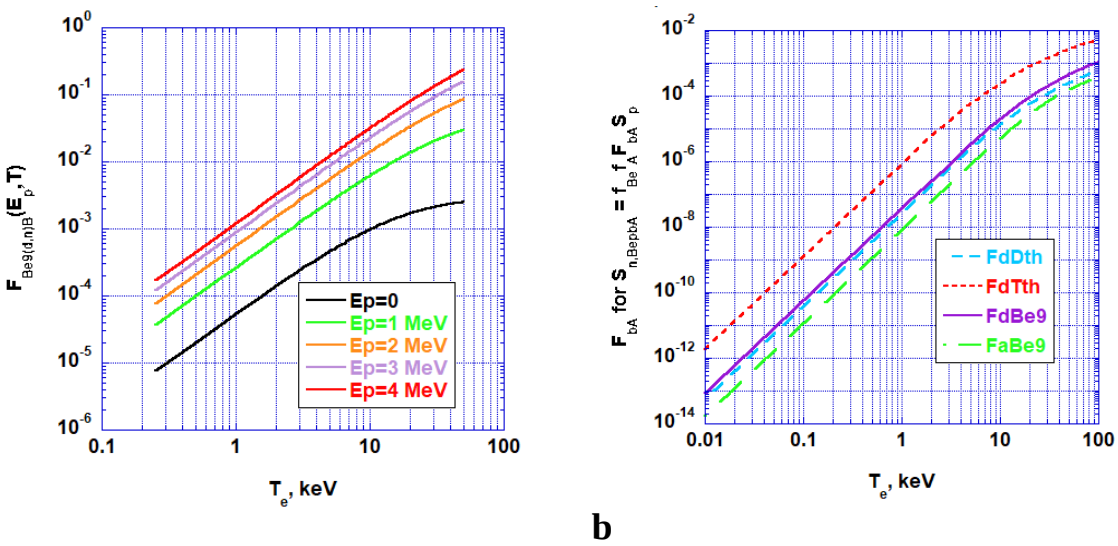


**a** **b**

*Figure 2. (a) Probability of the secondary reaction $^9$Be (d,n)B leading to neutron production between beryllium and fast deuterium originated from primary reaction $^9$Be(p,d)2$\alpha$ versus electron temperature, $T_e$, for different energies of protons, $E_p$, and (b) Neutron production probability by a fast protons originated from the NBI with $E_p$ =870 keV through secondary processes mediated by fast d and $\alpha$ (fast-d with thermal d, fast-d with thermal T, fast-d with beryllium and fast-$\alpha$ with beryllium) as a function of electron temperature averaged over the slowing down distribution functions of fast p, d and $\alpha$ with A=$D_{th}$,$T_{th}$,, $^9$Be, b= d, $\alpha$ .*

The probability that a fast proton leads to neutron production through a secondary fast particle (deuteron or alpha) is thus a weak function of plasma composition (through $v_c$), and depends mainly on the electron temperature:

$$\{F_{n,Bepb}(T)\} = \int_0^{v_b} \frac{\tau_{sp} n_e}{v^3+v_{cp}^3} \sigma_{Bepb}(E_p) F_{bBe}(E_p,T) v_p^3 dv_p, \qquad (14)$$

$\sigma_{Bepb}(E_p)$ is the cross section for the reaction of fast proton with beryllium leading to the production of fast particle *b*.

The total neutron sources through these secondary processes can be expressed as:

$$S'_{n,Bepb} = S'_p(E_b) f_{Be}^2 \{F_{n,Bepb}(T)\}. \qquad (15)$$

The probability of the secondary reactions through fast *d*, $F_{dBe}(E_p,T)$ and the associated neutron production for $H^0$-NBI with energy $E_b = 870\ keV$, $\{F_{n,Bepb}(T)\}$ for $b = d,\alpha$ are presented in Fig. 2 (a), (b) respectively.

Transport of the thermal ion species is simulated in a 1.5D approximation described in section 3. The densities of suprathermal deuterons and alphas are calculated in the slowing down approximation.

The density of the supra-thermal deuterons or alphas with energy $E_b$ is given by:

$$n_b(E_b) = S'_p(E_b)\tau_{sb} \ln(1+(\frac{v_b}{v_c})^2)/3. \qquad (16)$$

where $E_b$ is the birth energy of the fast deuteron or alpha particles. For the general case of a fast proton distribution, not necessarily describable by the slowing down approximation, the fast b density for a given temperature is given by:

$$n_b(T) = c_{Be} \int_0^\infty \int_{-1}^1 f_p\left(T_e, E_p, \mu\right) d\mu \sigma_{Bepb}(E_p) K_{nb}\left(E_p, T\right) v_p^3 dv_p, \quad (17)$$

with

$$K_{nb}\left(E_p, T\right) = n_e \tau_{sd} \int_0^\pi \ln(1 + (\frac{v_{b(E_p,\vartheta)}}{v_c})^2)\, d\vartheta/3\pi\,, \quad (18)$$

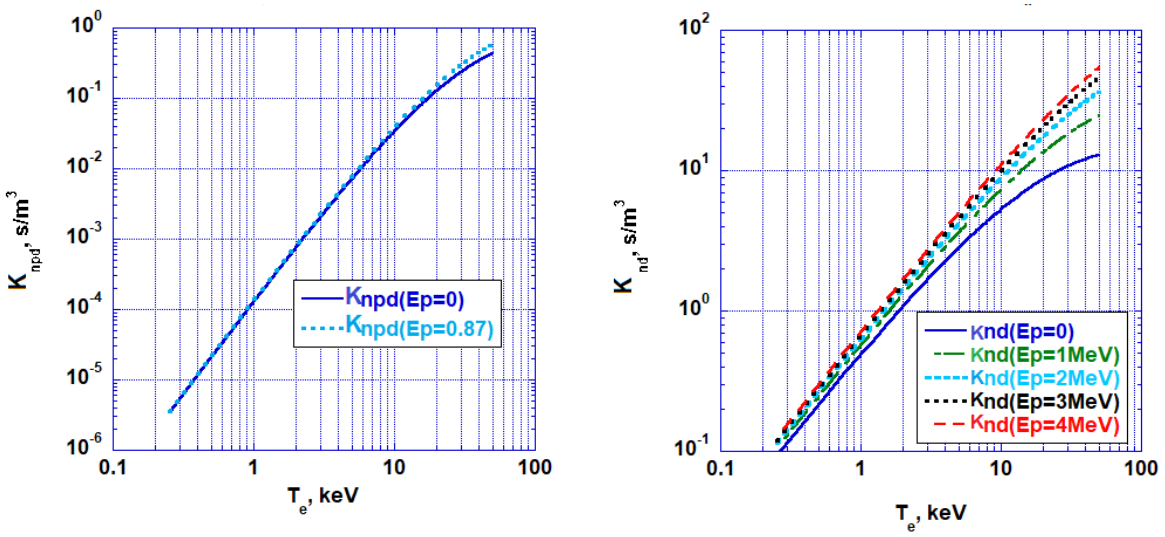


**a** **b**

*Figure 3. Impact of the fast deuterium spectrum on the fast deuteron density: (a) total impact (18) for the $H^0$-NBI with $E_p$= 870 keV with $K_{npd}=n_d n_{e19}/S_p/c_{Be}$; (b) partial impact (16) for higher energy protons, accelerated by the ICRH with $K_{nd}=n_d n_{e19}/S_d(E_3(E_p))$.*

where $\mu = (\vec{v} \cdot \vec{B})/vB$, $(\vec{v} \cdot \vec{B})$ is the scalar product of $\vec{v}$ and $\vec{B}$. If we consider $H^0$-NBI heating without ICRH, for which the slowing down approximation of fast protons is valid, this becomes:

$$n_b(T) = S_p'(E_p) c_{Be} n_e^{-1} K_{npb}\left(E_p, T\right), \quad (19)$$

with

$$K_{npb}(E_b, T) = \int_0^{v_b} \frac{\tau_{sp} n_e}{v^3 + v_{cp}^3} \sigma_{Bepb}(E_p) K_{nb}\left(E_p, T\right) v_p^3 dv_p. \quad (20)$$

The functions $K_{nb}\left(E_p, T\right), K_{npb}\left(E_p, T\right)$ for $E_p = 870\ keV$ and $b$=$d$ are shown in Fig. 3.

For slowing fast deuterons and a slowing down fast proton distribution function the impact of the fast *d* spectra on the fast *d* density is relatively small (see Fig. 3 (a). On the contrary, a higher impact is expected for high temperature plasmas with ICRH heating leading to higher proton energies (Fig. 3 (b)).

The cross-sections and probabilities of the reactions discussed above were used in the following assessment of neutron production at pre-DT phase of the ITER Research Plan by simulations with the ASTRA and TORIC-SSFPQL codes.

## 3. Transport simulations

To model neutron production in these plasmas we model the particle densities, $n_e$, $n_D$, $n_T$, temperatures, $T_i$, $T_e$, and current density, $j$, profiles with 1.5D transport simulations performed with the Automated System for Transport Analysis (ASTRA) [9] applying the boundary

conditions predicted by SOLPS parameterisation [14]. Plasma impurity concentrations ($c_i \equiv n_i/n_e$), such as $c_{Be}$ , $c_{Ne}$, and minorities for ICRH heating ($c_{He3}$, $c_H$ (in He) ) are prescribed as constants. The main ion densities, $n_H$ or $n_{He}$ are calculated from quasi-neutrality conditions, $n_e = \sum_i Z_i n_i$. Heat diffusivities, $\chi_i$=$\chi_e$, are fitted at the Edge Transport Barrier (ETB) to provide the value of the pedestal pressure, $p_{e,ped}$, predicted by EPED1+SOLPS [14]. For the core, heat diffusivities, $\chi_i$=$\chi_e$, are fitted to provide the energy confinement expected for hydrogen H-mode plasmas according to the $H_{y2,98}$ scaling ($\tau_{Hy2,98}$~ $A_i^{0.19}$ for $A_i = \frac{m_i}{m_p} = 1$), $\tau_E$= $\tau_{Hy2,98}$ ($A_i$=1), and $\tau_E$= $\tau_{L,97}$ ($A_i$=1), for L-mode operation [15] and this value is also used for helium plasmas. Particle diffusivities, $D_d = D_t$, for the reaction products (thermal deuterium and tritium) are fitted to provide a particle confinement to energy confinement ratio of $\tau_p$ = *10* $\tau_E$. The plasma fuelling rate is adjusted to provide plasmas with densities at about half of the Greenwald density, $n_e \approx 0.5\, n_G$, with $n_G = I_p/\pi a^2$, $[10^{20} m^{-3}, MA, m]$, which are typical of PFPO plasmas [1].

Two maximum ECRH power levels have been considered, the baseline power, $P_{EC} = 20\ MW$, and higher level, $P_{EC} = 30\ MW$, which is being studied as a possible early upgrade to the baseline.

Hydrogen Neutron Beam Injection ($H^0$-NBI) is modelled by [4-5] with a combination of 16.5 *MW* on-axis and 16.5 *MW* off-axis NBIs, with maximum beam energy, $E_p = 870\ keV$.

Ion Cyclotron Resonance Heating (ICRH) with a power up to $P_{IC} = 20\ MW$, and range of frequencies, $f_{IC} = 40 - 55\ MHz$ is modelled consistently by TORIC-SSFPQL suite of codes [6], including synergies with NBI.

Impact of saw-tooth (ST) and TAE on fast particles and neutron rate is modelled by instant mixing of plasma parameters (for saw-tooth) and fast ion redistribution within the central zone of radius $X_{ST}$. Here we use as a spatial variable *X*, a square root of the normalised toroidal magnetic flux. We assumed that the mixing area is connected with the location of *q*=1 resonance surface by Kadomtsev-like relation, $X_{ST}$ = 1.4 *X*(q=1). The moment of the ST crash corresponds to appearance of the resonance surface *q*=1 due to current profile evolution. To evaluate the maximum impact of TAEs on fast ions we use the instant mixing within the radius affected by TAEs, which appeared to be within the radius close to $X_{ST}$ (see section 6).

The results of simulations of helium and hydrogen L-and H-mode plasmas in PFPO are discussed in the next section.

## 4. Neutron production in PFPO helium and hydrogen plasmas with NBI and ECRH

The mechanisms of neutron production in helium and hydrogen plasmas are related to the background presence of residual deuterium in hydrogen (0.015 % deuterons per proton) and to the interaction of fast protons from the NBI with beryllium impurities in the plasma. The residual deuterium can react with itself producing 2.45 MeV neutrons and tritium. The tritium can further react with deuterium and produce 14 MeV neutrons. Since the natural level of deuterium is so low in hydrogen, whenever the plasmas are heated by NBI the production of deuterium by fast proton impact on beryllium can dominate and, thus, not only the fast proton beryllium processes depend on the concentration of beryllium but also the DD and DT neutron production reactions. This also applies to helium plasmas, in which no residual deuterium is

naturally present, that can produce DD and DT neutrons through the secondary processes resulting of fast proton beryllium interactions. Table 1 shows the results of the modelling of neutron sources and resulting D and T in a helium 7.5 MA/ 2.65 T plasma heated with NBI, which is expected to be performed in PFPO-2, for a range of beryllium concentrations.

**Table 1. Neutron and fast particle production for a helium H-mode plasma with $I_p$/B= 7.5 MA/2.65 T. All sources are given in $s^{-1}$.**

| $c_{Be}$, % | $S_{n14}$ | $S_{n2.45}$ | $S_{Be(d,n)X}$ | $S_{Be(\alpha,n)X}$ | $S_{Be(p,d)2\alpha}$ | $S_{Be(p,\alpha)Li}$ | $c_D$% | $c_T$% |
|---|---|---|---|---|---|---|---|---|
| 1 | 3.66 $10^4$ | 1.95 $10^9$ | 9.1 $10^{11}$ | 2.6 $10^{11}$ | 1.81 $10^{16}$ | 2.2 $10^{16}$ | 0.00202 | 1.1 $10^{-10}$ |
| 2 | 2.05 $10^5$ | 5.7 $10^9$ | 3.6 $10^{12}$ | 1.03 $10^{12}$ | 3.6 $10^{16}$ | 4.6 $10^{16}$ | 0.00326 | 4.1 $10^{-10}$ |
| 5 | 2.5 $10^6$ | 2.98 $10^{10}$ | 2.18 $10^{13}$ | 6.25 $10^{12}$ | 8.9 $10^{16}$ | 1.15 $10^{16}$ | 0.006 | 1.65 $10^{-9}$ |
| 7 | 6.1 $10^6$ | 5.37 $10^{10}$ | 4.14 $10^{13}$ | 1.18 $10^{13}$ | 1.23 $10^{17}$ | 1.58 $10^{17}$ | 0.008 | 3.2 $10^{-9}$ |
| 10 | 1.7 $10^7$ | 1.04 $10^{11}$ | 8.30 $10^{13}$ | 2.36 $10^{13}$ | 1.80 $10^{17}$ | 2.2 $10^{17}$ | 0.011 | 6.5 $10^{-9}$ |

The data in the table correspond to helium plasma heated by ECRH and NBI ($P_{EC}$= 20 MW, $H^0$-NBI with $P_{NBI}$=33 MW, $E_p$ = 870 keV) with neon concentration of $c_{Ne}$=1%, and range of Be impurity concentrations. $S_{n14}$ is the DT 14 MeV neutron source, $S_{n2.45}$ is the 2.45 MeV DD source, $S_{Be9(d,n)X}$ is the neutron source from reaction (2), $S_{Be9(p,d)2\alpha}$ is the fast deuteron production from reaction (1), $S_{Be(\alpha,n)X}$ is the neutron source from reaction (6), $S_{Be(p,\alpha)Li}$ is the fast alpha production from reaction (5) and $c_{Be}$, $c_D$, and $c_T$ are the concentrations of beryllium , deuterium and tritium in the plasma (in %).

The production of deuterium, $S_{Be(p,d)2\alpha} \sim c_{Be}$ and thus production of secondary neutrons by the sequence of reactions (1)-(2), $S_{Be(d,n)X} \sim c_{Be}^2$. In these He plasmas the concentration of thermal deuterium scales as $c_D \sim S_{Be(p,d)2\alpha} \sim c_{Be}$ and, thus, the source of tritium and 2.45 MeV neutrons scales as, $S_t \approx S_{n2.45} \sim S_{Be(p,d)2\alpha} n_D \sim c_{Be}^2$, while the 14 MeV neutron production scales as, $S_{n14} \sim S_t n_T \sim c_{Be}^3$. For high concentration of beryllium in helium plasmas the deuterium concentration can reach the same level as that of natural deuterium in hydrogen~ $10^{-4}$. It should be noted that reaction (3) leading to neutron production by direct proton-beryllium interactions does not occur in these plasmas because it has a threshold energy which is much higher than the one of the fast protons injected by ITER's NBI system (870 keV) (Fig. 1).

To provide an upper limit to tritium and neutron production in the PFPO phase we have modelled a range of plasmas heated with NBI and ECRH, which are foreseen to be explored in this phase including both hydrogen and helium L-mode and H-mode plasmas, assuming a beryllium concentration of 10%. This is a conservative assumption, since this value is more than factor of 2 higher than the typical levels measured during JET operation ($c_{Be}$ ~ 1%) with an ITER-like beryllium wall and a tungsten divertor [16]. The results of our study are summarized in Table 2.

**Table 2. Neutron and fast particle production for a hydrogen and helium plasmas. All sources are given in $s^{-1}$.**

| $A_i/I_p/B$/ mode -/ MA/T/- | $P_{EC}/P_{NBI}$ MW | $S_{n14}$ | $S_{n2.45}$ | $S_{Be(d,n)X}$ | $S_{Be(\alpha,n)X}$ | $S_{Be(p,d)2\alpha}$ | $S_{Be(p,\alpha)Li}$ |
|---|---|---|---|---|---|---|---|
| 1/5/1.8/H[1)] | 20/10.5 | 5.7 $10^5$ | 1.05 $10^{10}$ | 1.9 $10^{13}$ | 6.07 $10^{12}$ | 1.46 $10^{16}$ | 1.9 $10^{16}$ |
| 4/5/1.8/H[2)] | 20/8.3 | 5.4 $10^4$ | 9.1 $10^8$ | 6.16 $10^{12}$ | 1.55 $10^{12}$ | 1.19 $10^{16}$ | 1.55 $10^{16}$ |
| 4/7.5/2.65/H | 20/33 | 1.7 $10^7$ | 1.07 $10^{11}$ | 8.3 $10^{13}$ | 2.36 $10^{13}$ | 1.8 $10^{17}$ | 2.2 $10^{17}$ |
| 1/7.5/2.65/H | 20/33 | 5.7 $10^6$ | 6.5 $10^{10}$ | 8. $10^{13}$ | 2.7 $10^{13}$ | 7.6 $10^{16}$ | 1. $10^{17}$ |
| 1/5/2.65/L[3)] | 20/8.3 | 1.1 $10^5$ | 3.8 $10^9$ | 6.03 $10^{12}$ | 3.81 $10^{12}$ | 1.17 $10^{16}$ | 1.53 $10^{16}$ |
| 1/7.5/2.65/L | 20/33 | 5.7 $10^5$ | 1.85 $10^{10}$ | 2.24 $10^{13}$ | 5.91 $10^{12}$ | 6.7 $10^{16}$ | 8.5 $10^{16}$ |
| 1/7.5/2.65/L | 10/16.5 | 2.0 $10^5$ | 6.8 $10^9$ | 8.5 $10^{12}$ | 2.15 $10^{12}$ | 2.9 $10^{16}$ | 3.7 $10^{16}$ |

| | | | | | | | |
|---|---|---|---|---|---|---|---|
| 1/15/5.3/L | 20/33 | $1.8\ 10^{6}$ | $2.99\ 10^{10}$ | $2.8\ 10^{13}$ | $7.7\ 10^{12}$ | $7.5\ 10^{16}$ | $9.6\ 10^{16}$ |
| 1/15/5.3/L | 10/16.5 | $3.1\ 10^{6}$ | $1.34\ 10^{10}$ | $1.28\ 10^{13}$ | $3.45\ 10^{12}$ | $3.6\ 10^{16}$ | $4.6\ 10^{16}$ |
| 1/10/5.3/L | 20/33 | $1.4\ 10^{6}$ | $3\ 10^{10}$ | $3.03\ 10^{13}$ | $8.22\ 10^{12}$ | $7.9\ 10^{16}$ | $1.\ 10^{17}$ |
| 1/10/5.3/L | 10/16.5 | $5.1\ 10^{5}$ | $1.13\ 10^{10}$ | $1.2\ 10^{13}$ | $3.16\ 10^{12}$ | $3.5\ 10^{16}$ | $4.5\ 10^{16}$ |
| 1/10/5.3/L | 10/0 | $5.7\ 10^{3}$ | $2.6\ 10^{8}$ | 0 | 0 | 0 | 0 |
| 1/10/5.3/L | 20/0 | $1.1\ 10^{4}$ | $3.5\ 10^{8}$ | 0 | 0 | 0 | 0 |
| 1/7.5/2.65/L | 10/0 | $1.5\ 10^{3}$ | $7.5\ 10^{7}$ | 0 | 0 | 0 | 0 |
| 1/7.5/2.65/L | 20/0 | $2.0\ 10^{3}$ | $9.7\ 10^{7}$ | 0 | 0 | 0 | 0 |
| 1/5/2.65/L | 20/0 | $1.9\ 10^{2}$ | $1.18\ 10^{7}$ | 0 | 0 | 0 | 0 |
| 1/5/2.65/L | 10/0 | $1.6\ 10^{2}$ | $1.16\ 10^{7}$ | 0 | 0 | 0 | 0 |
| 1/5/1.8/H | 20/0 | $2.1\ 10^{2}$ | $3.7\ 10^{7}$ | 0 | 0 | 0 | 0 |

The data in the table correspond to L-mode and H-mode heated with ECRH and NBI for a range of conditions to be explored in the PFPO phase of the IRP for a beryllium concentration of $c_{Be}$ = 10 %. The maximum NBI energy is 870 keV providing 16.5 MW per injector. The rest of notations are the same as in the Table 1.The neon concentration was varied, $c_{Ne}$ = 0.2 – 1%, to maintain acceptable divertor loads for the chosen operational density.

For the cases [1)], [2)] the plasma density was increased and the NBI energy was reduced to provide acceptable shine-through loads on the first wall: [1)] $E_p$ = 550 keV, $n/n_G \sim 0.54$, [2)] $E_p$ = 500 keV, $n/n_G \sim 0.65$.[3)] H-mode operation at $I_p/B$ = 5/2.65 MA/T in hydrogen is unlikely absence of good absorption ICRH scheme [17] and the shinethrough constraints, implying the necessity to reduce NBI voltage to its lowest value $E_b$ = 500keV. This results in a total input power which is below the L-H power threshold in hydrogen $P_{NBI}(n_{shine}) + P_{EC}$ =28.3 MW < $P_{LH,H}(n_{shine})$.

Note that, without NBI heating, neutron production in hydrogen plasmas is solely due to the presence of 0.015% of deuterium due to the finite hydrogen purity and that the DD and DT neutron sources are several orders of magnitude lower than when $H^0$-NBI heating is used to heat the plasma. For helium plasmas without NBI heating there is no residual deuterium and the neutron production is zero; these helium plasmas to be explored in PFPO are not included in Table 2.

## 5. Neutron emission for helium and hydrogen operation with NBI, ECRH and ICRH

According to the IRP [1], it is foreseen to explore H-mode operation at 2.65 T plasmas in PFPO-2. Given the available heating power and the expected H-mode threshold for hydrogen and helium plasmas, this exploration is likely to be performed in helium since, this species provides a wider operational space in H-mode. In PFPO-2, the full baseline additional heating power will be available, comprising $H^0$-NBI with energy, $E_p$ = 870 keV, $P_{NBI}$= 33 MW, ECRH at $f_{EC}$ = 170 GHz with $P_{EC}$= 20 MW.

At the PFPO-2 phase it is suggested also to use the ICRH with frequencies in the range $f_{IC}$ = 40-53 MHz and $P_{IC}$ = 20 MW. Use of ICRH requires individual consideration of the neutral yield for each of foreseen heating schemes. Here we consider different antenna phasing using for IC heating and IC current drive, ICRH in the minority heating scheme with different species (H, $^3$He), individual ICRH and combination of the ICRH with the NBI, as well as 3-ion heating scheme [18, 7]. All these heating schemes have different impacts on the neutron yield producing different sorts of fast ions with different fast ion energy spectra.

Note that for $B_0$ = 2.65 T the ICRH at frequencies $f_{IC}$ ~ 40 MHz correspond to having the fundamental ion-cyclotron resonance of hydrogen, $\omega = \omega_{ci}(H)$ close to the plasma center $R \sim 6$ m. For these helium plasmas, it is possible to add a small amount of hydrogen ($c_H \sim \approx$ 5-10%) to perform ICRH heating of H-minority ions. When ICRH H-minority heating is applied together with NBI, the presence of the NBI suprathermal hydrogen ions affects the absorption profiles of ICRH power and the shape of the distribution function of the fast protons in the velocity space [3]. This, in turn strongly affect the intensity of the nuclear reactions involving Be impurity with protons and deuterons. We have simulated the synergetic impact of NBI and ICRH on the fast proton distribution using coupled TORIC and SSFPQL with NBI sources [6] as described in the reference [3] with the toroidal wave number of the spectrum peak corresponding to the dipole ($\pi$) and current-drive ($\pi/2$) antenna phasings.

The results of the simulations of fusion products are summarized in Table 3 and illustrated in Figs. 4, 5. We find that the impact of the synergy between $H^0$-NBI and H-minority ICRH on neutron production is strongly nonlinear. This is the result of the widening of the ICRH profile due to absorption on the fast protons injected by NBI, mentioned above and shown in Fig. 5a, as well as due to higher hydrogen minority density in presence of the NBI, leading to very different fast proton distributions (see Fig. 5.b).

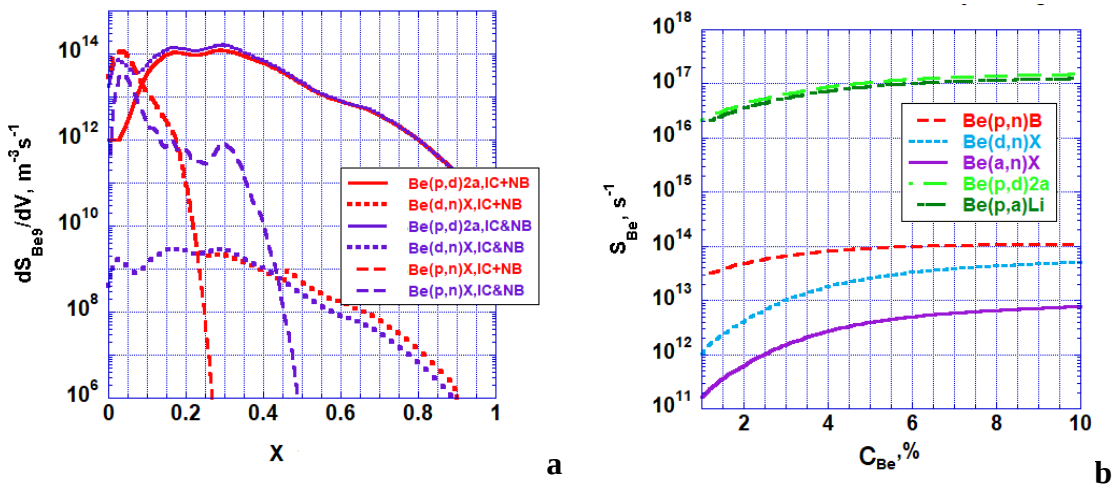


*Figure 4 (a) Radial distribution of the reactivity for reactions (1),(2) for 7.5 MA/2.65 T ITER helium plasmas with 20 MW of ECH, 33 MW of NBI and 20 MW of ICRH hydrogen minority heating with $c_H$ = 5% with and $c_{Be}$ = 1%, assuming linear superposition of NBI and ICRH (IC+NB) and including synergistic effects (IC&NB) and (b) Dependence of the fusion rates for reactions (1)-(3),(5),(6) on concentration of beryllium impurity.*

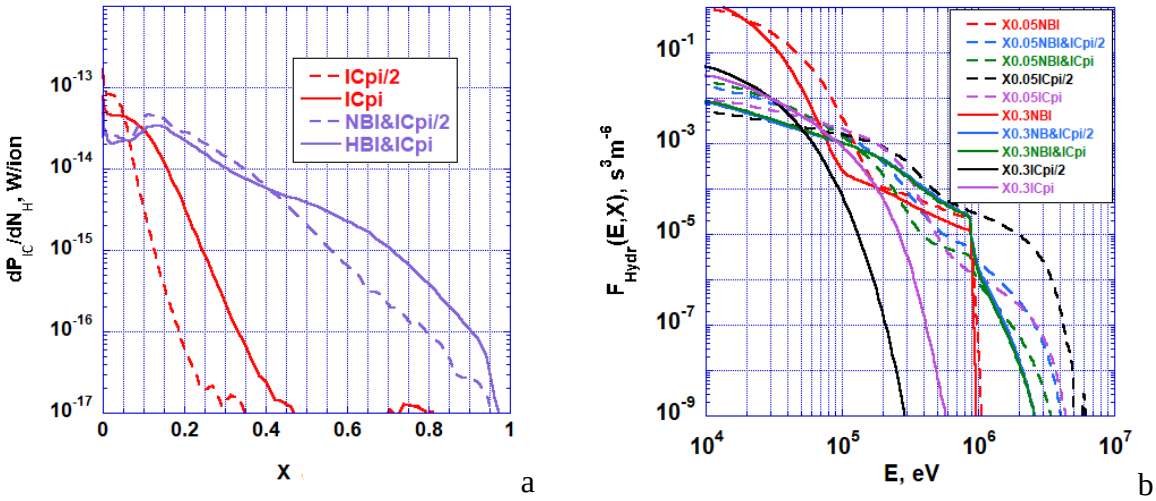


*Figure 5 (a) Radial distribution of the ICRH power absorption per ion for 7.5 MA/2.65 T ITER helium plasmas with NBI and ICRH hydrogen minority heating with $c_H$ = 5% with and $c_{Be}$ = 1%, with and w/o NBI for different phasing of the ICRH antennas. (b) Fast hydrogen distribution vs. ion energy at X=0.05 and X=0.3 radial locations for the same cases in (a). X corresponds to the square root of the toroidal magnetic flux.*

Our simulations show that ICRH accelerated hydrogen minority have a higher energy for current drive phasing as compared to the dipole phasing. It is caused by higher power per particle absorbed by minority protons at central region accelerating more particles to higher energies (Fig. 5b) and thus producing more neutrons (cf. Fig. 1). Presence of fast protons from the NBI strongly increases absorption of the ICRH power at the outer plasma regions thus reducing penetration to the centre. This strongly reduces the number of fast protons in the range 2-5 MeV and thus neutron production from $^9$Be(p,n)X reactions (see Fig. 1). It is important to note that the neutron source $S_{\mathrm{Be(p,n)X}}$ driven by H-minority accelerated protons by ICRH dominates over the whole range of Be concentrations in the majority of heating schemes with ICRH. This is due to the fact that there is a significant number of fast protons with energies in the range of 2-5 MeV accelerated by ICRH where the cross section for this reaction has comparable values to the secondary ones and, since this is a primary process, the densities of the two reacting species are larger.

**Table 3. Neutron and fast particle production for 7.5 MA/2.65 T helium H-mode plasmas. All sources are given in $s^{-1}$.**

| N | $P_{NBI}/P_{IC}$(phase) | $S_{\mathrm{Be(p,n)X}}$ | $S_{\mathrm{Be(d,n)X}}$ | $S_{\mathrm{Be(\alpha,n)X}}$ | $S_{\mathrm{Be(p,d)2\alpha}}$ | $S_{\mathrm{Be(p,\alpha)Li6}}$ |
|---|---|---|---|---|---|---|
| 1 | 33/20 MW($\pi$/2) | 4.92 $10^{14}$ | 1.12 $10^{14}$ | 1.76 $10^{13}$ | 2.26 $10^{17}$ | 1.90 $10^{17}$ |
| 2 | 33/20 MW($\pi$) | 9.68 $10^{13}$ | 9.96 $10^{13}$ | 1.46 $10^{13}$ | 2.09 $10^{17}$ | 1.75 $10^{17}$ |
| 3 | 0/20 MW($\pi$/2) | 3.40 $10^{15}$ | 3.82 $10^{13}$ | 1.10 $10^{13}$ | 4.58 $10^{16}$ | 4.15 $10^{16}$ |
| 4 | 0/20 MW($\pi$) | 8.20 $10^{13}$ | 4.58 $10^{12}$ | 4.45 $10^{11}$ | 1.04 $10^{16}$ | 8.41 $10^{15}$ |
| 5 | 33/0 MW | <<1 | 8.29 $10^{13}$ | 1.18 $10^{13}$ | 1.81 $10^{17}$ | 1.51 $10^{17}$ |

The data in the table correspond to the plasmas heated with 20 MW of ECRH, and a combination of ICRH and NBI, with a beryllium concentration of $c_{Be}$ = 10 % and a range antenna phasings. The maximum NBI energy is 870 keV providing 16.5 MW per injector. The rest of notations are the same as in the Table 1.

As mentioned before, hydrogen H-mode operation at 2.65 T is unlikely due the high H-mode power threshold, partly also due to the lack of an efficient ICRH heating scheme, the operational space of hydrogen H-mode plasmas in ITER has been recently re-analyzed, taking into account the addition of ~10% helium in these plasmas [20]. In JET-ILW experiments, adding a small amount of $^4$He ions in hydrogen plasmas was shown to result in a significant reduction of the H-mode power threshold [19]. The operational space of hydrogen H-mode plasmas in ITER has been recently re-analyzed [20] and a promising operational scenario at somewhat higher $B_0$ = 3.0-3.3T in predominantly hydrogen plasmas with the addition of ~10-15% helium was proposed [21]. Under these conditions, H + ~10% $^4$He mixed plasmas in ITER can be additionally efficiently heated with 20 MW of ICRH power using the 3-ion scheme and a very small amount of $^3$He ions ($c_{He3}$ < 1%) to absorb ICRH power at the high-field side off-axis [21]. The efficiency of the 3-ion $^4$He-($^3$He)-H ICRH scheme with off-axis $^3$He resonance for plasma heating and triggering ELMs in H-$^4$He plasmas was recently demonstrated on the ASDEX Upgrade [22].

Figure 6 shows the location of the ion cyclotron resonance layer for $^3$He ions for the application of the 3-ion ICRH scheme in ITER H + ~10% $^4$He plasmas. At $B_0$ = 3.0-3.3T, the L-H threshold will increase by 10-20% in comparison with 2.65T operation. Yet this scenario allows to deliver additionally 20 MW of ICRH power for plasma heating, which in combination with NBI and ECRF makes H-mode operation possible in predominantly hydrogen plasmas in ITER. As demonstrated on JET, the 3-ion ICRH scenario in large tokamaks allows to use extremely low amounts of $^3$He, e.g. $c_{He3}$ ~ 0.1% for efficient plasma heating [7]. The results of the simulations of the 3-ion scheme for a 8.8 MA / 3.12 T hydrogen plasma with $c_{He4}$ = 15%, $c_{He3}$ = 0.1% and $c_{Be}$ = 1% are shown in Tab. 4 and Figs. 7(a). In these simulations 20 MW of ICRH at $f_{IC}$ = 40 MHz was considered and the fast ions produced by 33 MW of H$^0$-NBI with $E_p$= 0.87 MeV were also accounted for. Fast $^3$He ions generated by ICRH lead to the neutron production through reaction (4). Figure 7(b) shows the increase in the neutron production from the reactions between ICRH-generated $^3$He ions and $^9$Be impurities with increasing $c_{Be}$, which is lower than the neutron rate production in helium plasmas with H minority ICRH (see Table 3).

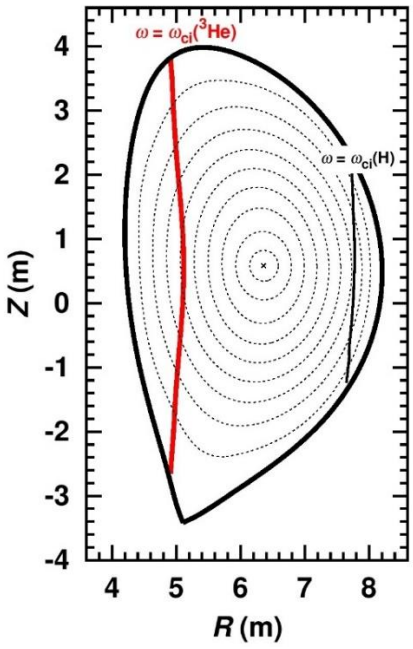


For the considered 3-ion ICRH scenario in PFPO plasmas, Be impurities at the level of ~1% do not impact significantly the propagation and absorption of ICRH waves and the range of $^4$He concentrations for efficient ICRH heating is fairly large, $c_{He4} \approx$ 5 - 17%. However, at significantly higher Be concentrations, these impurities also substantially contribute to the RF polarization, similarly to $^4$He ions. The relation 6 $c_{He4}$ + 10$c_{Be} \leq 1$ defines the range when ICRH heating of $^3$He ions with the 3-ion scheme can be made effective in PFPO-2 plasmas. This relation can be derived using the procedure described in [18], by extending the plasma composition to include four ions species (H, $^4$He, $^9$Be and $^3$He). At very large concentrations of $^9$Be impurities $c_{Be} \approx$ 9-10%, no injection of $^4$He ions is required for the application of the 3-ion ICRH scheme because $^9$Be takes over the role of $^4$He for impacting the RF polarization.

.

*Figure 6. Location of the ICRH resonant layer for $^3$He. Note that the absorption of the RF takes place at r/a = 0.6-0.7.*

**Table 4. Neutron and fast particle production for 8.8 MA/3.11 T hydrogen-dominant H-mode plasmas. All sources are given in $s^{-1}$.**

| $S_{n14}$ | $S_{n2.45}$ | $S_{Be(He3,n)X}$ | $S_{Be(d,n)X}$ | $S_{Be(\alpha,n)X}$ | $S_{Be(p,d)2\alpha}$ | $S_{Be(p,\alpha)Li6}$ | $S_{Be(p,n)X}$ |
|---|---|---|---|---|---|---|---|
| $3.45\ 10^{7}$ | $1.8\ 10^{11}$ | $4.8\ 10^{14}$ | $1.12\ 10^{14}$ | $1.73\ 10^{13}$ | $2.08\ 10^{17}$ | $1.73\ 10^{17}$ | $1.9\ 10^{12}$ |

The data in the table correspond to a hydrogen plasma heated with 20 MW of ECRH, 33 MW NBI ($E_p$ = 870 keV), 20 MW ICRH with heating ($\pi$) phase configuration and containing 0.1% $^3$He and 15% $^4$He and 1% Be. The rest of notations are the same as in the Table 1.

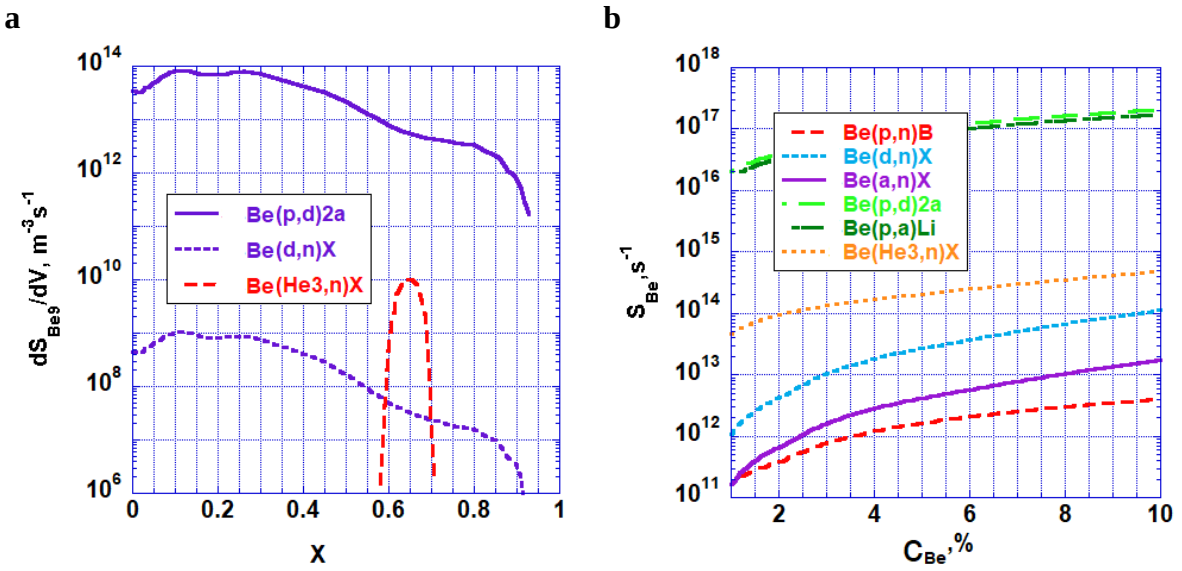


*Figure 7. (a) Radial profiles of the reactivity for reactions (1), (2) and (4) for a hydrogen dominant 8.8 MA/ 3.12 T H-mode plasma with 20 MW ECRH, 33 MW NBI and 20 MW ICRH 3-ion scheme heating with $c_{He3}$ = 0.1% , $c_{He4}$ = 5%, $c_{Be}$=1%, $E_p$ = 870 keV; (b) Dependence of the reaction rates for reactions (1)-(6 on the concentration of beryllium impurity.*

The IRP [1] also foresees the testing of the conventional ICRH $^3$He minority heating scheme during PFPO-2 in hydrogen plasmas at full-field. Since the auxiliary heating power of 73MW is below the L-H threshold for hydrogen plasmas at B=5.3T, the plasmas in which this scheme will be demonstrated will be L-modes. Similar to 3-ion scheme we have assessed the dependence of neutron production on the concentration of beryllium impurity $c_{Be}$ self-consistently by modelling the ICRH power absorption with the fast ion distributions with the TORIC-SSFPQL code. The results are summarized in Tab. 5 and Fig 8.

**Table 5. Neutron and fast particle production for 15 MA/5.3 T hydrogen L-mode plasmas. All sources are given in $s^{-1}$.**

| $c_{Be}$, % | $S_{n14}$ | $S_{n2.45}$ | $S_{Be(d,n)X}$ | $S_{Be(\alpha,n)X}$ | $S_{Be(p,d)2\alpha}$ | $S_{Be(p,\alpha)\ Li6}$ | $S_{Be(He3,n)X}$ |
|---|---|---|---|---|---|---|---|
| 1 | $1.2\ 10^{5}$ | $5.9\ 10^{9}$ | $3.53\ 10^{11}$ | $5.49\ 10^{10}$ | $8.85\ 10^{15}$ | $7.4\ 10^{15}$ | $5.5\ 10^{12}$ |
| 10 | $4.1\ 10^{6}$ | $4.12\ 10^{10}$ | $3.55\ 10^{13}$ | $1.\ 10^{13}$ | $8.4\ 10^{16}$ | $1.08\ 10^{17}$ | <<1 |

The data in the table correspond to the plasma heated with 20 MW of ECRH, 33 MW NBI ($E_p$= 870 keV), 20 MW ICRH with heating ($\pi$) phase configuration with 3% $^3$He. The rest of notations are the same as in the Table 1.

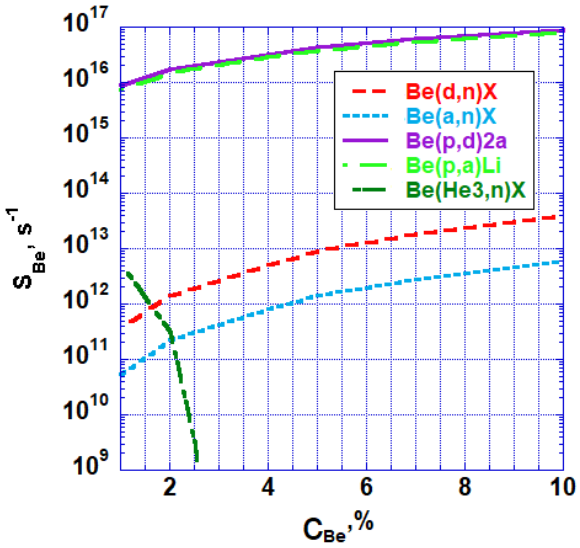


*Figure 8. Dependence of the reaction rates for reactions (1),(2) and (4)-(6) on the concentration of beryllium impurity for 15 MA/5.3 T hydrogen L-mode plasmas heated with 20 MW of ECRH, 33 MW NBI ($E_p$ = 870 keV), 20 MW ICRH with heating ($\pi$) phase configuration with 3% $^3$He.*

Our studies shows that for $^9$Be concentrations of about 1%, an efficient absorption ICRH power can be achieved with $^3$He concentrations of ~3% in these 15 MA/5.3T plasmas. However for higher Be concentrations (4-5%) the predicted neutron production due to fast $^3$He impact on beryllium decreases strongly. This is due to a strong decrease in the Single Pass Absorption (SPA); in such plasmas, the wave propagation is characterized by the presence of the ion-ion hybrid evanescence layer, preventing a direct access of ICRF waves to the cyclotron resonance of $^3$He minority ions. At these high Be concentrations, the fast waves are strongly reflected from the evanescence layer, leading to a strong amplification of RF electric fields at the plasma edge. Under these conditions, non-linear edge mechanisms of ICRH power absorption play an important role and, for this reason, the $^3$He minority scheme does not provide efficient ICRH heating of the bulk plasma.

Therefore, for high $^9$Be concentrations, we have also studied the 3-ion ICRH scheme with $^3$He minority at low concentrations (< 1%). The presence of intrinsic $^9$Be impurities and additionally injected $^4$He ions can be applied to optimize the left-hand RF polarization in the vicinity of the cyclotron resonance of $^3$He minority ions. Depending on the amount of $^9$Be impurities in the plasma, the level of $^4$He ions has to be chosen accordingly to:

$$c_{He4} \approx (0.5\text{-}1.0)\, c_{He4,ref} \quad (21)$$

$$c_{He4,ref} = (1 - 10c_{Be})/6 \quad (22)$$

Note that for a given level of $^9$Be, good ICRH absorption by $^3$He ions can be achieved for a fairly broad range of $^4$He concentrations. In fact, if $c_{Be}$ gets as high as ~ 8-10%, there is no need for extra $^4$He for an efficient ICRH heating of $^3$He minority ions.

Fig. 9 compares the modelled neutron production in 15 MA/5.3T hydrogen (or hydrogen-dominant) plasmas heated by the $^3$He minority and the 3-ion schemes. For the 3-ion scheme

simulations we have considered an extremely low $^3$He content, $c_{He3}$=0.1%. For such low $c_{He3}$, the $^3$He fast-ion energies and the rate of the corresponding nuclear reactions, $S_{Be(He3,n)X}$ are maximized. Neutron production with the 3-ion scheme can be reduced by increasing the concentration of $^3$He minority ions (e.g., ~0.5-1%), varying the $^4$He concentration to make a broader absorption profile by $^3$He ions or by shifting the $^3$He cyclotron resonance out of magnetic axis (decreasing the magnetic field) to decrease the absorbed power density and temperature.

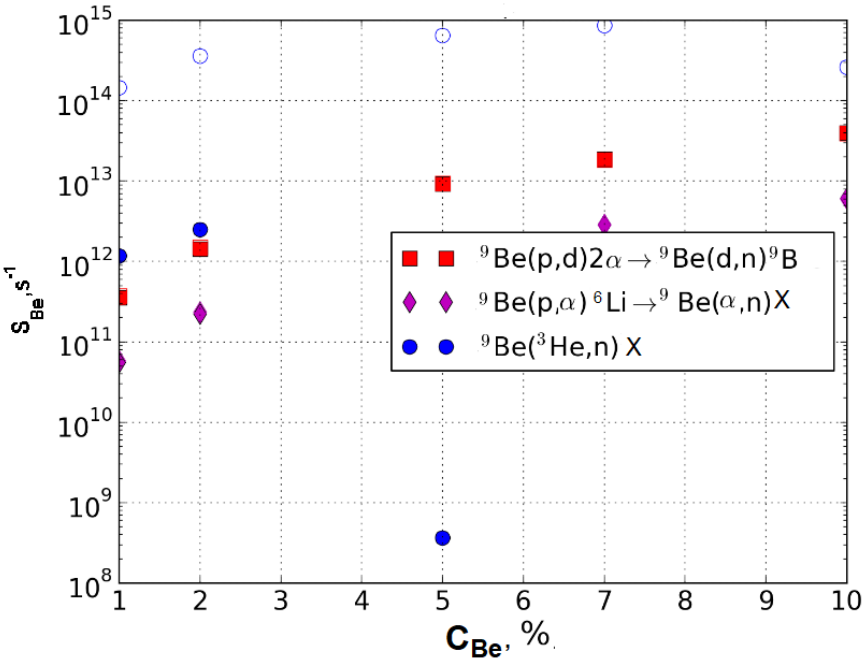


*Figure 9. Neutron production rate as a function of the $^9$Be concentration for the 15 MA/5.3 T hydrogen-dominant L-mode plasmas in ITER heated with 20 MW of ECRH, 33 MW NBI ($E_p$ = 870 keV), 20 MW ICRH (dipole phasing). Full symbols correspond to the $^3$He minority scheme with $c_{He3}$ = 3%, whereas the open symbols correspond to the 3-ion ICRF scheme with $c_{He3}$ =0.1%.*

## 6. Impact of TAE modes and saw-teeth on neutron yield

As already shown in [24], the 7.5 MA/2.65 T plasmas with high heating power in PFPO-2, required to access the H-mode in He (and possible hydrogen) plasmas, have a wide zone of weak or weak reversed magnetic shear, and high fraction of supra-thermal ion pressure, $\beta_{fast}/\beta_{th}$ ~ 20 - 25%, with peaked pressure profile, $p_0/<p>$ ~ 3 - 4 (Fig. 10) as a consequence of the effective current drive and fast proton densities provided by NBI heating in these plasma conditions, where the brackets <…> are used for volume averaged values. Such peaked fast ion profiles can potentially cause the excitation of TAE instabilities, which in turn can cause the redistribution of fast particles and, therefore, modify the neutron production.

To determine the plasma scenarios where the excitation of TAEs is more probable, we evaluate the maximum effect TAEs will have on EP profiles by studying the scenarios foreseen for the PFPO-2 phase. In our consideration, we use the atomic units for the ion mass, expressing $M_i$ in the mass of proton, $M_p$: $A_i = M_i/M_p$.

The Alfven velocity can be expressed as follows:

$$V_A = 2.18\ 10^6\ B/(n_{i20}A_i)^{1/2} = 2.18\ 10^6\ B\ (Z_i/n_{20}A_i)^{1/2}\ ,\ [\text{m/s, T, } 10^{20}\text{m}^{-3}] \qquad (23)$$

Here we use the equation of quasi-neutrality for the main ion: $n = n_e \approx Z_i n_i$

The ion beam velocity can be expressed as follows:

$$E_b = 1.38\ 10^7\ (E_b/A_b)^{1/2}, \text{ [m/s, MeV]}. \quad (24)$$

where $E_b$ is the NBI energy.

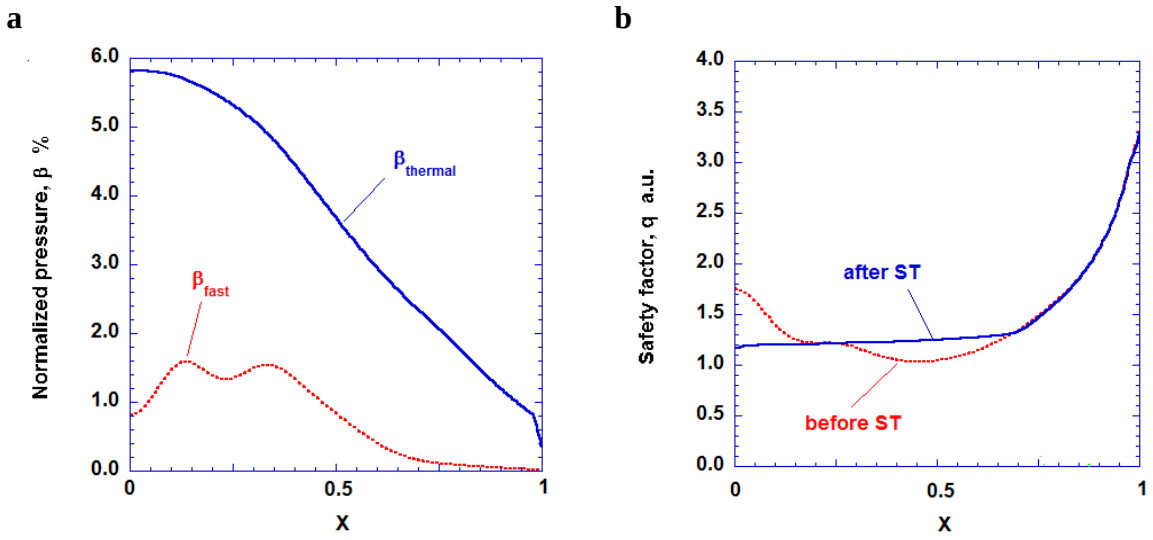


*Figure 10. 7.5 MA/2.65 T helium H-mode plasma with 33 MW of $H^0$-NBI and 20 MW ECR heating and <n>=3.5 $10^{19}m^{-3}$: (a) fast and thermal pressure profiles. (b) Safety factor profile before and after a saw-tooth crash.*

We introduce the Superalfvenic index, which characterizes the ratio of the beam ion velocity to the Alfvenic one:

$$F_{Ab} = V_b/V_A = 6.67\ B^{-1}(Z_i A_b/A_i E_b n_{20})^{-1/2} = 3.58\ (aB)^{-1}(Z_i A_b/A_i E_b g I_p)^{-1/2}, \quad (25)$$

where $I_p$ [MA] is the plasma current, a[m], is the plasma minor radius and $g$ is the Greenwald density fraction, $g = \frac{n}{n_G} = 0 - 1$. For typical ITER NBI heated plasmas with $a$ = 2 m, $E_b$= 0.87 MeV, $A_b$= 1, and expressing plasma current through the edge safety factor, $q_{95}$, where $B/I_p \sim q_{95}$= 3 for $B$ =5.3 T, $I_p$=15 MA, we get the following expression

$$F_{Ab} = 1.22\ ((Z_i/A_i)(q_{95}/3)(B/5.3)/g)^{-1/2}, \text{ [T]} \quad (26)$$

where for PFPO in hydrogen plasmas $Z_i/A_i$ = 1 and in helium plasmas $Z_i/A_i$ = 0.5. Note that the value of the density corresponding to the minimum power to access the H-mode can be expressed for ITER as $n/n_G(P_{LH}(n) = P_{LH,min}) \equiv g_{LH} \approx 0.35\ (q_{95}/3)^{2/3}$ [25].

Tab. 6 summarizes the values of the Superalfvenic index for range of hydrogen plasma conditions to be explored in PFPO-2 with $q_{95}$ = 3 and a range of densities (from $n/n_G = g_{LH}$ to $n/n_G$ = 1). Note that a chosen value of the field, $B$, the value of the Supralfvenic index at high density $F_{Ab}(g$ =1) decreases with plasma current as $F_{max} \sim I_p^{0.5} \sim q_{95}^{-0.5}$ . On the other hand, the value at low density $F_{Ab}(n/n_G = g_{LH})$ is less sensitive to the plasma current, $F_{min} \sim I_p^{0.17} \sim q_{95}^{-0.17}$.

To obtain the corresponding values for He plasmas with the same electron densities it is necessary to multiply the hydrogen values by $(A_i/Z_i)^{1/2} \sim 1.41$.

Thus, the plasma conditions in which NBI ions are superalfvenic correspond to high density 7.5 MA/2.65 T Helium H-mode plasmas. Note that for helium plasmas with hydrogen NBI the superalfvenic index is about 20% higher than for the DT plasma with deuterium NBI foreseen in FPO (assuming that other parameters are the same) ($F_{Ab} \sim (A_i/A_b/Z_i)^{0.5}$).

**Table 6. Superalfvenic index for the ITER hydrogen and helium plasmas in PFPO=2.**

| $B$, T | 5.3 | | 3.3 | | 2.65 | | 1.8 | |
|---|---|---|---|---|---|---|---|---|
| $n/n_G$ | 0.35 | 1 | 0.35 | 1 | 0.35 | 1 | 0.35 | 1 |
| $F_{Ap,H}$ | 0.73 | 1.22 | 0.92 | 1.54 | 1.03 | 1.72 | 1.25 | 2.11 |
| $F_{Ap,He}$ | 1.03 | 1.72 | 1.3 | 2.17 | 1.45 | 2.53 | 1.76 | 2.97 |

Note that full NBI energy may not be used in practice for 1.8 T plasmas due excessive shine-through loads on ITER's first wall.

Linear Alfven stability analysis of these ITER plasmas has been carried out using the NOVA/NOVA-K suite of codes [26,24]. The ideal MHD code NOVA finds the Alfvenic mode structures, which are then used for stability calculations by NOVA-K. These codes have been extensively validated against other similar models and include the most significant driving and stabilizing mechanisms important for Alfven mode physics [27]. The driving term includes the finite orbit and finite Larmor radius effects while the damping terms include: ion and electron Landau damping, TAE radiative damping, and trapped electron collisional damping.

The results of stability analysis for the ITER 7.5 MA/2.65 T helium H-mode plasma with 33 MW of $H^0$-NBI and 20 MW ECRH heating with $n/n_G$ = 0.5 (see Fig. 10) leading to $F_{Ap,He}$ ≈1.8 is shown in Fig. 10, which is close to the most unstable case $F_{Ab} \sim 2$ [11].

The NOVA simulations predict that the unstable TAE modes are localized within the low/WRS zone $X < 0.5$. Excitation of such modes can have a large effect on the strongly peaked neutron source due to the fast ion densities in this region resulting from central ICRH and NBI heating in PFPO-2 plasmas (note that in the case studied here we only consider fast protons from NBI). Another important effect of this TAE instability is the modification of the NBI current drive due to fast proton redistribution, which requires detailed knowledge of the phase space of the redistributed ions compared to the one before the instability is triggered.

Modelling of the impact of the saw-tooth oscillations on the fast particle redistribution and the neutron production by fast particle-beryllium interactions has been carried out with the ASTRA code including a time-dependent version of the fast ion Fokker-Planck solver [4]. The saw-tooth and TAE impact on fast particles redistribution and neutron production has been modelled by mixing of the plasma parameters (saw-tooth) and redistribution the fast ions within the mixing radius for the saw-teeth ($X_{ST}$ = 1.4 $X$(q=1)) for saw-teeth, and with $X = X_{TAE}$ determined by the Alfven mode instability region for Alfvenic modes. The period of saw-teeth is determined by the resistive time for the central zone of the plasma (~ 10 s) when the $q$ profile evolves back to the saw-tooth triggering conditions. The period of TAE instabilities is determined by fast particle slowing down time when the fast particle distribution evolves back

to the TAE triggering conditions. The results of the simulations including both fast ion redistribution effects are shown in Fig. 11.

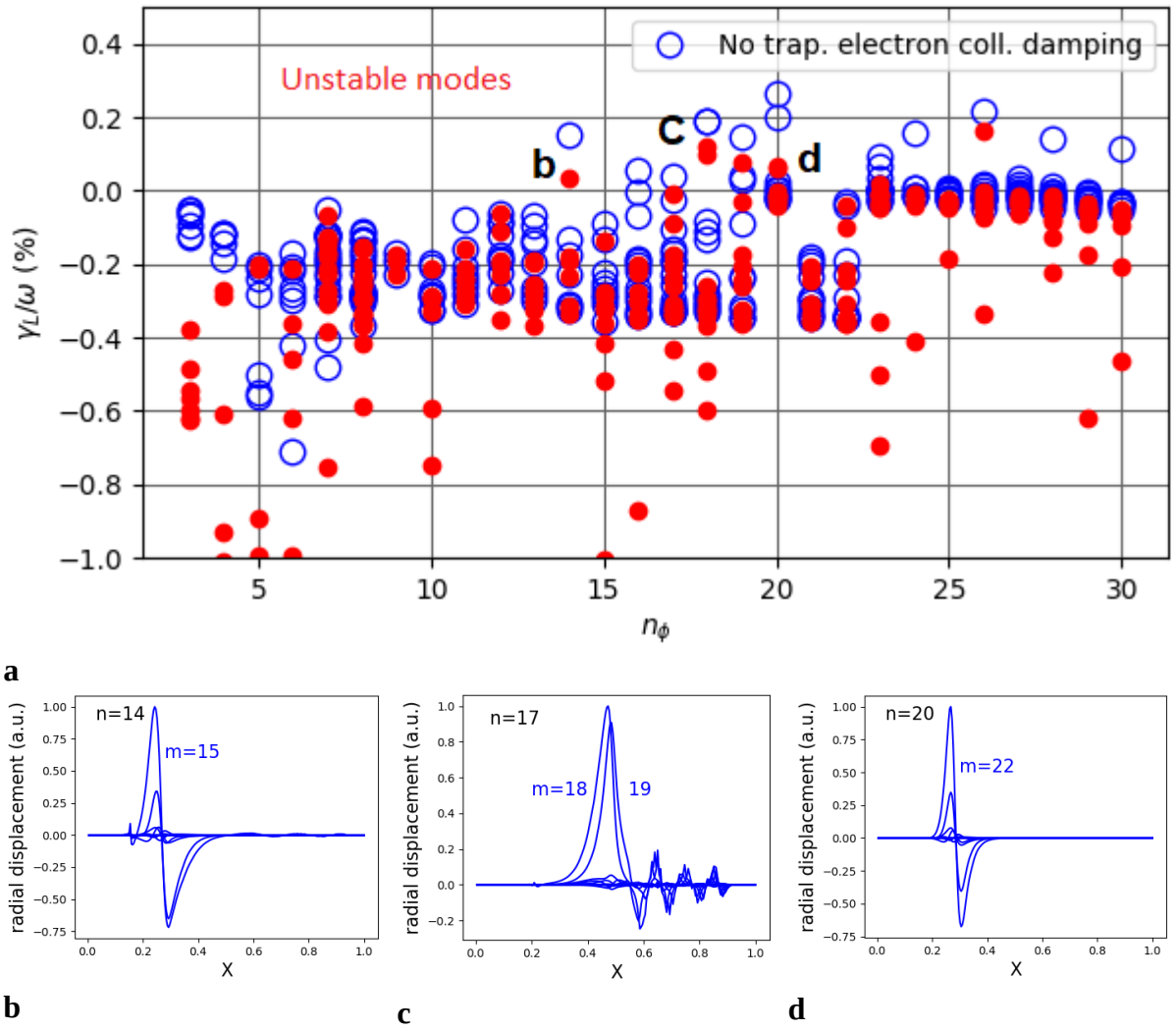


*Figure 11. (a) Linear growth rates for unstable TAE modes versus toroidal mode numbers for an ITER 7.5 MA/2.65 T helium H-mode plasma at $n/n_G$ = 0.5 with 33 MW of $H^0$-NBI and 20 MW ECRH heating. (b), (c), (d) Three most unstable representative TAE radial structures for the same plasma conditions.*

The effect of the saw-teeth on the total neutron production are found to be small since the fast ion distribution recovery time of $\tau_S$ ~ 1 s is much smaller than the resistive time that dictates saw-tooth repetition times, $\tau_{ST}$ ~ 10 s. On the other hand, the reduction of the neutron source due to TAEs is much larger and can decrease it by more than 30%. This effect is expected to be even more significant for ICRH hydrogen minority ions and its evaluation is the topic of further studies.

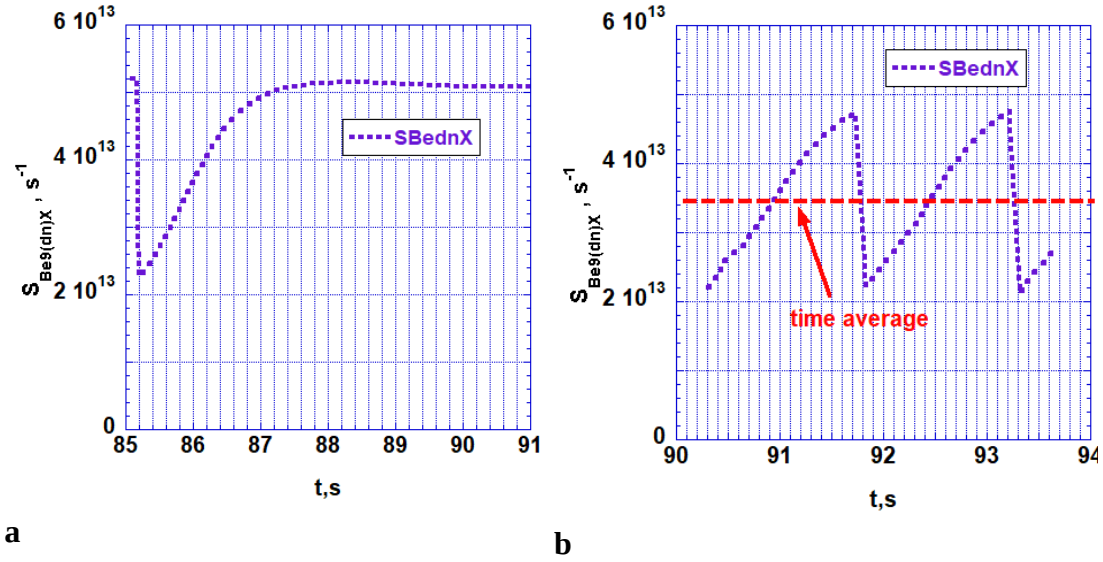


*Figure 12. Impact of saw-tooth (a) and TAE induced (b) mixing of fast particles on the neutron rate for an ITER 7.5 MA/2.65 T helium H-mode plasma at $n/n_G$ = 0.5 with 33 MW of $H^0$-NBI and 20 MW ECRH heating with $c_{Be}$ = 10%.*

## 7. Discussion and conclusions

The experimental evidence of the importance of nuclear reactions between Be impurities and fast particles produced by auxiliary heating schemes was demonstrated in JET measurements [25, 2, 26]. In particular, γ-ray diagnostics for energetic ions based on reaction (2) are discussed in ref. [28]. Observation of neutron production by reaction (4) during $^3$He minority heating is reported in ref [2]. Evidence of $^9$Be - p nuclear reactions during second harmonic majority and hydrogen minority ICRH in JET-ILW hydrogen and deuterium plasmas is described in [29]. This has triggered our evaluation of the magnitude of such neutrons producing reactions in the PFPO phase of the IRP where hydrogen and helium plasmas will be explored.

For the PFPO-1 phase, where plasmas will only be heated by ECRH, the only source of neutrons is the residual deuterium in the natural hydrogen and the magnitude of the neutron source is low (zero for helium plasmas). For the PFPO-2 phase, where ICRH and NBI will also be available, the main source of neutrons is caused by interaction of Be impurities with the primary supra-thermal ions produced by ICRH and NBI and with the secondary fast particles (d,α) produced by the interaction of the primary ions with beryllium (Be(p,d)2α , Be(p, α)Li) that then further react with beryllium impurities producing neutrons.

The neutron production rates for the plasma conditions to be explored in PFPO with NBI and ICRH heating are in the range of $10^{12}$ – 5 $10^{14}$ n/s assuming that the beryllium concentration in the plasma can reach values of up to 10%. For plasmas heated with ECRH only the neutron production rates are several orders of magnitude lower (zero for helium plasmas). The highest values of the neutron rates in PFPO correspond to H-mode heated plasmas with ICRH for which a sizeable fast ion tail is produced. It is important to note that these neutron productions rates are several orders of magnitude lower than those expected even in DD plasmas at ITER, for which typical rates are ≤ $10^{18}$ n/s, this upper value being achieved for 15 MA/5.3 T DD plasmas with 73 MW of auxiliary heating). Note that our simulations for ITER 15 MA ICRH heated plasmas with $^3$He and 2-5% Be concentration predict similar neutron rates (~ 6 $10^{14}$ n/s, c.f. Fig. 9) to those of [2] but the corresponding $^3$He concentrations that produce these rates is

lower in our modelling than in [2], since we consider self-consistently simulated plasma conditions.

Neutron production in NBI (or NBI+ECRH) heated plasmas is solely produced through secondary processes since the energy of the protons generated by the ITER NBIs ($E_p \leq 870$ keV) is lower than the threshold energy for direct neutron-production reactions with beryllium. Since the secondary neutron production processes scale as ~ $c_{Be}^2$, the neutron production by these mechanisms that will eventually occur in ITER plasmas is likely to be much smaller than our estimates here where we have assumed a 10% beryllium concentration, in contrast with the 1-2% typical of JET operation with the ITER-like Wall [16].

For PFPO-2 with ICRH heating, the processes leading to neutron production by fast particle interaction with beryllium and their dependences on beryllium concentration are more complex. This is due to different fast minority distributions being produced for different antenna phasings and the modifications to the ICRH absorption and the resulting fast particle distribution densities and energies. In all cases with ICRH, the dominant sources of neutron production are the direct reactions of ICRH accelerated minorities (H or $^3$He) with beryllium, since there is a substantial amount of fast particles with higher energy than the threshold energies of the direct reactions of the minorities with beryllium. For simultaneous applications of ICRH and NBI, the presence of the fast protons from the NBI, on which the ICRH is preferentially absorbed, reduces the number of high energy protons in the distribution thus leading to a lower neutron production than the linear combination of the independent NBI and ICH sources. Similarly, the dependence of the neutron emission with beryllium concentration with ICRH heated plasmas is not always linear, as in the case of NBI. This is due to ICRH absorption effects related to Be that can lead to saturation of the neutron source with increasing beryllium concentration (hydrogen minority at 2.65 T) and even to a decrease due to poor absorption ($^3$He minority at 5.3 T).

It is important to note that the production of neutrons in PFPO is also strongly affected by the local plasma parameters, such as the temperature, that have a large impact on fast particle slowing down and thus on the number of fast ions with sufficient energy to react with beryllium. This allows flexibility to decrease this production during the commissioning of the NBI and ICRH systems by carrying out this commissioning in L-mode plasmas at high densities and thus lower temperatures and thus smaller number of fast ions with high energies. For example, the 3-ion ICRH scheme for PFPO-2 studies is characterized by the off-axis resonance location ($X \approx 0.65$), leading to a decrease of the absorbed RF power density. In combination with lower plasma temperature in the absorption region and shorter slowing-down time, this results in a lower neutron production in 8.8 MA/3.1T predominantly hydrogen plasmas with the 3-ion ICRH scheme as compared to the neutron generation with central H minority ICRH in helium plasmas at 7.5 MA/2.65 T

Our modelling has also shows that the local fractions of NBI and ICRH fast ion pressures and their gradients in PFPO-2 H-mode plasmas are similar or even higher (for 7.5 MA/2.65 T He H-mode plasmas) than those of fast alphas in the ITER Q = 10 baseline scenario. This makes AEs unstable in the wide plasma region with low magnetic shear, r/a< 0.5, typical in these plasmas due to the very effective NBI current drive.

We have modelled the effect of saw-teeth and AEs on the neutron rate due to the fast particle redistribution that they cause. We have found that saw-teeth can noticeably modify the local

neutron production across the plasma cross section but do not affect much the total neutron production from the plasma. On the contrary, AEs can cause a significant reduction of the neutron rate more than 30%. This difference between saw-teeth and AEs is due to magnitude of the timescale for recovery of the fast ion distribution compared to the MHD instability repetition time. For saw-teeth, the fast ion distribution recovers in timescales much shorter than the saw-tooth repetition time, while for AEs the two timescales are similar.

It is important to note that there remain uncertainties that need to be resolved to refine the neutron production estimates presented here. First, the cross-sections for the fast ion-beryllium reactions considered are not very accurate in the ITER-relevant range of energies and further modelling and experimental work to refine their values is needed. In addition, as mentioned above, the neutron production rate depends nonlinearly on the local electron temperature, which impacts the fast ion distribution, and on the Be concentration. The values for the plasma parameters considered in our study are modelled by adjusting the values of the transport coefficients to reproduce the plasma energy expected from scalings for ITER. If the values of the plasma temperature in ITER were to deviate strongly from those predicted by the scalings, or if the beryllium concentration were much lower than assumed here, the neutron production associated would be significantly different from the values presented here.

*Disclaimer: ITER is the Nuclear Facility INB no. 174. The views and opinions expressed herein do not necessarily reflect those of the ITER Organization. This publication is provided for scientific purposes only. Its contents should not be considered as commitments from the ITER Organization as a nuclear operator in the frame of the licensing process.*

## References

[1] ITER Research Plan, ITER Technical Report ITR-18-03 ([1] "ITER Research Plan within the Staged Approach" (Level III – Provisional Version). ITER Technical Report ITR-18-003, 17 September 2018)
[2] M. Gatu Johnson et al Nucl. Fusion 50 (2010) 045005
[3] R. Bilato, et al, "Synergies between H-NBI fast-ions and ICRF heating in the non-activated operational phase of ITER", 45th EPS Conference on Plasma Physics, July 2-6, Prague, Check Republic, http://ocs.ciemat.es/EPS2018PAP/pdf/P1.1070.pdf
[4] A. Polevoi, et al "Benchmarking of the NBI block in ASTRA code versus the OFMC calculations", JAERI-DATA-Code 97-014, March 1997,
https://inis.iaea.org/collection/NCLCollectionStore/_Public/28/052/28052091.pdf
[5] A.R. Polevoi et al, "Reassessment of Steady State Operation in ITER with NBI and EC Heating and Current Drive", P5.1012, 46th EPS Conference on Plasma Physics, 8 - 12 July 2019, Milan, Italy, hppt://ocs.ciemat.es/EPS2019PAP/pdf/P5.1012.pdf
[6] R. Bilato, M. Brambilla, et al., Nucl. Fusion, 51 (2011) 103034
[7] Ye.O. Kazakov et al., *Nature Physics* **13**, 973-978 (2017)
[8] A.V. Zvonkov et al, Plasma Physics Reports, vol. 5, (1998) p. 389–400
[9] G.V. Pereverzev and P.N. Yushmanov, "ASTRA Automated System for TRansport Analysis in a Tokamak," Max-Planck IPP Report, vol. 5/98, 2002,
https://w3.pppl.gov/~hammett/work/2009/Astra_ocr.pdf
[10] G.Y. Fu, C.Z. Cheng, and K.L. Wong, Phys. Fluids B 5, 4040 (1993)
[11] N.N. Gorelenkov, C.Z. Cheng, and G.Y. Fu, Phys. Plasmas 6, 2802 (1999)
[12] A. Trkov, R.M. Capote Noy, A. Koning private communication (2019)
[13] H. Brysk, Plasma Phys. 15 (1973) 611, and references therein.
[14] A.R. Polevoi et.al., Nucl. Fusion 57 (2017) 02201

[15] ITER Physics Basis Nucl. Fusion 39 (1999) 2208
[16] Matthews, G.F., et al., Journal of Nuclear Materials 438 (2013) S2–S10
[17] E. Lerche et al, Plasma Phys. Control. Fusion 53 (2011) 124019.
[18] Ye.O. Kazakov et al., *Nucl. Fusion* **55**, 032001 (2015)
[19] J.C. Hillesheim et al., *Proc. 44th EPS Conf. Plasma Physics*, P5.162 (2017)
[20] B. Bigot et al., *Nucl. Fusion* **59**, 112001 (2019)
[21] M. Schneider et al., *EPJ Web Conf.* **157**, 03046 (2017)
[22] Ye.O. Kazakov et al., *Phys. Plasmas* **28**, 020501 (2021)
[23] Ye.O. Kazakov et al., *Phys. Plasmas* **28**, 020501 (2021)
[24] A.R. Polevoi, et al, "On Stability of ITER-like Plasma with High Fraction of Fast Ions.", P4.032 39th EPS Conference on Plasma Physics, Stockholm, Sweden, 2 - 6 July 2012
[25] F. Ryter, et al, Nucl. Fusion 54 (2014) 083003 (9pp)
[26] C.Z.Cheng, M.S.Chance Phys. Fluids, 29 (1986) 3695
[27] N. Gorelenkov et al., Nucl. Fusion, 45 (2005) 226
[28] V. G. Kiptily, et al, Nucl. Fusion 42 (2002) 999
[29] A.V. Krasilnikov, et al, Nucl. Fusion 58 (2018) 026033